BNL-81930-2009-BC

Theoretical Studies in Heterogenous Catalysis: Towards a Rational Design of Novel Catalysts for Hydrodesulfurization and Hydrogen Production

José A. Rodriguez and Ping Liu

To be published in "New Developments in QuantumChemistry"

October 2008

Chemistry Department

Brookhaven National Laboratory
P.O. Box 5000
Upton, NY 11973-5000
www.bnl.gov

DISCLAIMER

BNL-81930-2009-BC

Theoretical Studies in Heterogeneous Catalysis: Towards a Rational Design of Novel Catalysts for Hydrodesulfurization and Hydrogen Production

José A. Rodriguez and Ping Liu
Department of Chemistry
Brookhaven National Laboratory
Upton, New York 11973, USA

Introduction

Traditionally, knowledge in heterogeneous catalysis has come through empirical research [1,2]. Nowadays, there is a clear interest to change this since millions of dollars in products are generated every year in the chemical and petrochemical industries through catalytic processes [1-4]. To obtain a fundamental knowledge of the factors that determine the activity of heterogeneous catalysts is a challenge for modern science since many of these systems are very complex in nature [1,2]. In principle, when a molecule adsorbs on the surface of a heterogeneous catalyst, it can interact with a large number of bonding sites. It is known that the chemical properties of these bonding sites depend strongly on the chemical environment around them [1-4]. Thus, there can be big variations in chemical reactivity when going from one region to another in the surface of a heterogeneous catalyst [2,3-6]. A main objective is to understand how the structural and electronic properties of a surface affect the energetics for adsorption processes and the paths for dissociation and chemical reactions [3,4,7].

In recent years, advances in instrumentation and experimental procedures have allowed a large series of detailed works on the surface chemistry of heterogeneous catalysts [8-10]. In many cases, these experimental studies have shown interesting and unique phenomena. Theory is needed to unravel the basic interactions behind these phenomena and to provide a general framework for the interpretation of experimental results [3-7]. Ideally, theoretical calculations based on density-functional theory have evolved to the point that one should be able to predict patterns in the activity of catalytic surfaces [3,7]. As in the case of experimental techniques, no single theoretical approach is able to address the large diversity of phenomena occurring on a catalyst [7]. Catalytic surfaces are usually modeled using either a finite cluster or a two-dimensionally periodic slab [3-7]. Many articles have been published comparing the results of

these two approaches [5-7]. An important advantage of the cluster approach is that one can use the whole spectrum of quantum-chemical methods developed for small molecules with relatively minor modifications. On the other hand, the numerical effort involved in cluster calculations increases rather quickly with the size of the cluster [5]. This problem does not exist when using slab models. Due to the explicit incorporation of the periodicity of the crystal lattice through the Bloch theorem, the actual dimension of a slab calculation depends only on the size of the unit cell [3,7]. In practical terms, the slab approach is mainly useful for investigating the behavior of adsorbates at medium and high coverages. Very large unit cells are required at the limit of low to zero coverage, or when examining the properties and chemical behavior of isolated defect sites in a surface. In these cases, from a computational viewpoint, the cluster approach can be much more cost effective than the slab approach. Slab and cluster calculations can be performed at different levels of sophistication: semi-empirical methods, simple ab initio Hartree-Fock, ab initio post-Hartree-Fock (CI, MP2, etc), and density functional theory [3-7]. Density-functional (DF) based calculations frequently give adsorption geometries with a high degree of accuracy and predict reliable trends for the energetics of adsorption reactions [3,7].

This article provides a review of recent theoretical studies that deal with the behavior of novel catalysts used for hydrodesulfurization (HDS) reactions and the production of hydrogen (i.e. catalytic processes employed in the generation of clean fuels) [11-18]. These studies involve a strong coupling of theory and experiment. A significant fraction of the review is focused on the importance of size-effects and correlations between the electronic and chemical properties of catalytic materials [12,13,15-18]. The article begins with a discussion of results for the desulfurization of thiophene on metal carbides and phosphides, systems which have the potential to become the next generation of industrial HDS catalysts [19,20]. Then, systematic studies

concerned with the hydrogen-evolution reaction (HER) on extended surfaces, organometallic complexes and enzymes are presented [13]. Finally, the reasons for the high catalytic activity of Au-CeO_2 and Cu-CeO_2 in the production of hydrogen through the water-gas shift reaction (CO + H_2O → H_2 + CO_2) are analyzed [17,18]. It is shown that theoretical methods are very valuable tools for helping in the rational design of heterogeneous catalysts.

Hydrodesulfurization reactions on metal carbides and phosphides

Sulfur-containing compounds are common impurities in all crude oil [19,21]. In our industrial society, these impurities have a negative impact in the processing of oil-derived chemical feedstocks and degrade the quality of the air by forming sulfur oxides (SO_x) during the burning of fuels and by poisoning the catalysts used in vehicle catalytic converters [21]. Hydrodesulfurization (HDS) is one of the largest processes in petroleum refineries where sulfur is removed from the crude oil [19-22]. Most commercial HDS catalysts contain a mixture of MoS_2 and Ni or Co [22]. The search for better desulfurization catalysts is a major issue nowadays in industry and academic institutions [19-22]. Thus, it has been established that β-Mo_2C and other metal carbides are very active for the cleavage of C-S bonds, but their HDS activity decreases quickly with time [23]. The degradation of β-Mo_2C has been ascribed to the formation of a chemisorbed layer of sulfur or MoS_xC_y compounds on the surface of the catalyst [23].

DF calculations were used to study the interaction of atomic S and thiophene with extended α-Mo_2C(001) and MoC(001) surfaces and with a metcar Mo_8C_{12} nanoparticle [12,16]. Figure 1 shows the structure of these systems where the C/Mo ratio varies from 0.5, bulk Mo_2C, to 1.5, metcar Mo_8C_{12}. Structural and electronic effects determine the reactivity of the metal carbides [12,24]. In all of these systems there is a Mo → C charge transfer that varies as shown in the top

panel of Figure 2 [24]. The positive charge on Mo reduces electron-electron repulsion and leads to a negative shift (i.e. increase in stability) for the centroid of the Mo 4d band (see bottom panel in Figure 2). Neither the Mo → C charge transfer nor the stabilization of the Mo 4d band varies in a regular way with the C/Mo ratio in the carbide compounds [24]. Due to its structure, the metcar Mo_8C_{12} has special electronic properties [12,24].

DF calculations show a direct correlation between the charge on the Mo sites of the carbides and their ability to bind S and thiophene [12]. Figure 3 displays calculated S bonding energies. In the case of α-Mo_2C(001), the surface contains only Mo atoms and binds sulfur almost as strongly as pure Mo(110) [12,24]. The Mo→C charge transfer that exist in MoC(001) largely reduces the strength of the Mo-S bonds [12]. This trend in the reactivities of α-Mo_2C(001) and MoC(001) towards S have been verified by experimental measurements [11]. Thus, the full dissociation of hydrogen sulfide, $H_2S(gas) \rightarrow S(ads) + H_2(gas)$, is much faster on α-$Mo_2C$(001) than on MoC(001). At the same time, the removal of S by hydrogenation through the $H_2(gas) + S(ads) \rightarrow H_2S(gas)$ reaction at elevated temperatures is efficient on MoC(001) but not on α-Mo_2C(001) [11]. On this surface, the S atoms always adsorb at three-fold Mo sites. Interestingly, the S bonding energy becomes more and more exothermic when the S coverage on α-Mo_2C(001) increases from 0.25 to 1 ML. This can be seen as the prelude to the formation of a MoC_xS_y compound that eventually should induce the deactivation of Mo_2C in hydrodesulfurization reactions. According to Sabatier's principle, a good catalyst should bind the products or intermediates of a reaction in a moderate way. Thus, from the results in Figure 3, MoC is expected to be a better HDS catalyst than α-Mo_2C [11]. How efficient are these carbide compounds for the breaking C-S bonds?

Thiophene is a typical test molecule in HDS studies [1,2,19,22]. DF calculations show a very strong interaction between thiophene and the α-Mo_2C(001) surface [12]. The molecule adsorbs with its ring parallel to the surface and there is a spontaneous cleavage of a C-S bond (see Figure 4) [12]. Five Mo atoms of the α-Mo_2C(001) surface are involved in the bonding of the dissociated thiophene. Such a relatively large ensemble of metal atoms does not exist in a MoC(001) surface. The DF calculations show very weak bonding interactions between thiophene and MoC(001) [12]. The molecule is adsorbed via the S atom (see Figure 5) and there are very minor perturbations in its structural geometry. The calculated heat of adsorption is only 0.3 eV [12]. Results of x-ray photoelectron spectroscopy (XPS) have confirmed the DF predictions [11]. In experimental studies, the dissociation of thiophene on α-Mo_2C(001) was observed at temperatures between 150 and 200 K [11,25], whereas there was only weak chemisorption on MoC(001) without decomposition of the adsorbate [11].

Bulk α-Mo_2C and MoC will not perform well as HDS catalysts. One has serious problems for the dissociation of C-S bonds (MoC), and the other interacts too strongly with the main product of the HDS process (α-Mo_2C) [11]. Theoretical studies predict that metcar M_8C_{12} nanoparticles (M= Ti or Mo) should be better HDS catalysts, since they interact well with thiophene and do not bind S too strongly [15]. Figure 6 shows calculated structures for the thiophene + $3H_2$ → C_4H_8 + H_2S reaction on Ti_8C_{12}. In the first steps, a H_2 molecule dissociates over a C-C unit and then H atoms move to Ti sites. Upon interaction with thiophene, there are two successive hydrogenolysis of C-S bonds. In the final steps, the S deposited on the metcar reacts with hydrogen and H_2S evolves into gas phase. The corresponding calculated ΔE's and activation energies are displayed in Figure 7 [15]. The ruptures of the C-S bonds are exothermic reactions and energetically the most difficult steps involve the endothermic formation of H_2S

from S adatoms and hydrogen. The energy necessary for the last steps is released by the first steps of the HDS process [15]. The theoretical calculations indicate that the rate-limiting step for the HDS process on M_8C_{12} nanoparticles has an activation energy smaller than the corresponding one on a commercial Ni/MoS_2 catalyst [15].

Recently, transition metal phosphides have shown a tremendous potential as highly active HDS catalysts [20]. Among all the phosphides, Ni_2P/SiO_2 demonstrated the highest HDS activity (HDS conversion of 99%) and has been reported to be more efficient than NiMoS/Al_2O_3 (HDS conversion of 76%) [20,26,27]. Furthermore, Ni_2P does not deactivate with time as β-Mo_2C does [26]. The Ni_2P(001) surface is the predominant orientation observed in TEM images for Ni_2P/SiO_2 catalysts [27]. Along the [001] direction of Ni_2P, Ni_3P and Ni_3P_2 planes alternate to give the full stoichiometry of the bulk [28]. In DF calculations, the Ni_3P_2-terminated surface (Figure 8) was found to be more stable than a Ni_3P-terminated by 2.75eV/unitcell. This is consistent with the results of LEED and STM studies for Ni_2P(001) [11]. The surface in Figure 8 has well-defined ensembles of three metal atoms that are separated by ~ 3.8 Å [11,28]. Each cluster of nickel is surrounded by a group of six P atoms. DF studies indicate that the bonds in Ni_2P(001) are covalent in nature [11]. Although the s and d orbitals of Ni are mixed with the s, p orbitals of P, the valence bands in Ni_2P(001) exhibit strong metal d character, and the Ni atoms and P atoms of the surface are slightly charged (Ni: 0.07e; P: -0.07e). Experimental studies also point to a metallic behavior for Ni_2P [28]. Valence photoemission spectra for Ni_2P(001) show a valence band in which the Ni 3d levels mainly appear at 1 to 3 eV below the Fermi edge [28], as seen in calculated DOS plots [11].

Results of XPS experiments point to two types of adsorption sites for S on Ni_2P(001) at 300 K [11]. DF calculations indicate that the sulfur adatoms probably sit on the Ni three-fold hollow

sites of $Ni_2P(001)$ at low coverages. Under these conditions, the Ni-S bonds are strong. Ni-P bridge sites are probably populated at medium or large sulfur coverages. These Ni-P adsorption sites do not interact strongly with the adsorbate and are interesting because they allow the participation of P atoms in hydrodesulfurization reactions [11].

Overall the bonding of S on $Ni_2P(001)$ is not as strong as on α-$Mo_2C(001)$, and $Ni_2P(001)$ interacts better with thiophene than MoC(001) [11]. Figure 9 shows energy changes associated with the thiophene + $2H_2 \rightarrow C_4H_6 + H_2S$ reaction on $Ni_2P(001)$ [11]. This HDS process can be separated in two parts. First the cleavage of the C-S bonds, and second the hydrogenation of the hydrocarbon and S fragments of thiophene. The first part releases a large amount of energy that is then utilized to achieve the second part. The whole HDS process is exothermic. The very good catalytic performance reported for Ni_2P [20,26,27] can be ascribed to the moderate effects of Ni↔P interactions and the intrinsic reactivity of the P sites [11]. First of all, the "ligand effect" of P atoms on the Ni sites is relatively weak. The formation of Ni-P bonds produces a minor stabilization of the Ni 3d levels and the Ni→P charge transfer is very small. This leads to a reasonably high activity of Ni_2P to dissociate thiophene and hydrogen. Secondly, the active Ni sites of the surface decrease due to an "ensemble effect" of P, which prevents the system from the deactivation induced by high coverages of strongly bound S. In addition, P sites play an important role in the bonding of intermediates. When the Ni hollow sites are occupied by an adsorbate, the P sites can provide moderate bonding to the products of the decomposition of thiophene and the H adatoms necessary for hydrogenation [11]. Ni_2P is a highly active HDS catalyst by obeying Sabatier's principle: good bonding with the reactants, and moderate bonding with the products.

Hydrogen-evolution reaction on extended surfaces, organometallic complexes and enzymes

The hydrogen evolution reaction (HER) involves the conversion of protons and electrons into hydrogen gas ($2H^+ + 2e^- \rightarrow H_2$) at an electrode surface, and Pt is usually selected as the electrode catalyst [29]. With the hydrogen economy approaching, there has been a continuous search for more efficient and less expensive catalysts to replace Pt. Hydrogenase enzymes are quite interesting since they are able to catalyze the HER and its reverse with rapid rates at room temperature [30-33]. The behavior of the hydrogenases has also fueled intensive research aimed at the synthesis of close mimics that can achieve a comparable catalytic activity [30,34,35].

DF calculations were employed to describe the HER on the [NiFe] hydrogenase, plus the $[Ni(PS3^*)(CO)]^{1-}$ and $[Ni(PNP)_2]^{2+}$ complexes. Ni(111), Pt(111) and $Ni_2P(001)$ single crystal surfaces were also studied [13]. In general, a good HER catalyst should be able to trap protons and bond the atomic hydrogen strongly, while still desorb H_2. Figure 10 displays the relative energy changes for the HER on a series of catalysts, involving the sequential adsorption of two hydrogen atoms, followed by desorption of H_2 into gas phase. Accordingly, the better catalyst corresponds to that with energy changes closer to the zero energy line. One can see that Pt and Ni are two of the worst HER catalysts in the present study, corresponding to an energetics far away from the ideal zero line [36]. The atoms in Pt(111) and Ni(111) surfaces have a small negative charge (Pt:-0.1e; Ni:-0.05e). Therefore, shown in Figure 10, the first (H*) and second (2H*) hydrogen trapping on both metal surfaces are exothermic. As a result the recombination and removal of H_2 is the rate-limiting step (rls), which is too endothermic and the HER cannot proceed well.

In accordance with experiments [31-33], the DF calculations also show that the [NiFe] hydrogenase is superior to Pt as a HER catalyst. The first hydrogen atom has occupied a

positively charged Ni-Fe bridge site (see Figure 11). The second H prefers staying at the negatively charged terminal S of Cys492. This is the rls and the energy cost decreases to 0.2eV. The transition state corresponds to a dihydrogen sticking to the Ni sites, rather than the Fe sites. In contrast, the removal of hydrogen is exothermic. To interact with dihydrogen, the metal sites have to transfer electrons to hydrogen. Fe with a bigger positive charge does not bind dihydrogen as strongly as Ni. On the other hand, the coordination number of Fe is five, while Ni only has four ligands (see Figure 11) and therefore less steric repulsion towards dihydrogen. Overall, our calculations show that the Ni site of the hydrogenase plays an essential role in the HER. This is in agreement with experimental observations that point to Ni as the active site for the reaction with hydrogen [37,38].

Considering the activity of Ni sites under different chemical environments, it is of interest the HER on two Ni complexes, ($[Ni(PS3^*)(CO)]^{1-}$ and $[Ni(PNP)_2]^{2+}$), and the $Ni_2P(001)$ surface. The $[Ni(PS3^*)(CO)]^{1-}$ complex displays a HER activity that is much worse than that of the hydrogenase. The first H attacks the negatively charged S, accompanied by a spontaneous cleavage of a Ni-S bond and the formation of a HS group (see Figure 12). Similarly to the hydrogenase, the addition of the second H is the rls. With the decrease in the Ni coordination, the second H favors bonding to the positively charged Ni site. This is the rls and corresponds to a reaction energy (ΔE_{rls}) of 0.31eV, which is higher than that for the hydrogenase. In the case of $[Ni(PNP)_2]^{2+}$, the first bonded H favors the negatively charged N site (see Figure 13) rather than the positively charged Ni and P sites, while the second one prefers the Ni site rather than the N site. Accordingly, we propose a sequential migration of the bonded H from N to Ni ($[HNi(PNHP)_2]^{2+} \rightarrow [HNi(PNP)(PNHP)]^{2+}$). Note that the two H atoms have opposite charges. Therefore, once the migration is completed, the two H atoms attract each other and form a weak

H-H bond, a possible precursor for the formation of H_2. Similar to the Ni and Pt surfaces, the rls of the HER on $[Ni(PNP)_2]^{2+}$ is also the recombination and removal of hydrogen. However, in this case the energy cost is only 0.23eV.

As demonstrated above, when compared to the [NiFe] hydrogenase and its molecular analogues, bulk Pt or Ni catalyzes the HER less efficiently, as hydrogen bonds too strongly with the metals to be removed easily from the surface. The hydrogenase and its analogues include both a proton-acceptor (a negatively charged non-metal site) to strongly trap the protons, and a hydride-acceptor (usually the highly coordinated and isolated metal site) to provide moderate bonding to the hydrogen. With the cooperative function of these two kinds of sites, the [NiFe] hydrogenase displays a high catalytic activity in the HER. However, it has been found that under conditions different from their native environment, the [NiFe] hydrogenase may loss activity due to a lack of thermostability, which hinders the application of this enzyme or the Fe-only hydrogenase in industrial processes [39,40]. Therefore, Pt is still widely used as an industrial catalyst for the HER, [29] and there is a need to find a material that combines the catalytic activity of the [NiFe] hydrogenase and the thermostability of metal surfaces.

The $Ni_2P(001)$ system seems to meet the criteria of a good HER catalyst, combining the best features of surfaces, the [NiFe] hydrogenase and the molecular complexes. On one hand, $Ni_2P(001)$ (see Figure 14) is a solid surface as Pt(111) and Ni(111), and should have a higher thermostability than hydrogenase enzymes. In addition, due to the presence of the P atom in the surface, $Ni_2P(001)$ behaves somewhat like the hydrogenase rather than the pure metal surfaces. Both negatively charged P sites and positively charged Ni sites are present in the surface (ensemble effect). For the first hydrogen, the Ni hollow sites are highly preferred (see Figure 14). Due to a weak ligand effect [11], the deactivation of Ni atoms in the surface of $Ni_2P(001)$ is very

small and the Ni hollow sites are strong hydride-acceptors. As seen in Figure 10, the first H adsorption on $Ni_2P(001)$ is slightly weaker than that on Ni(111) but stronger than that on Pt(111), the hydrogenase and the molecular complexes. Different from the pure metal surfaces, the addition of the second atomic hydrogen is an endothermic process. This endothermicity is due to an ensemble effect. As shown in Figure 14, once the Ni hollow sites have been occupied, the additional adsorbate has to interact with the less active Ni-P bridge site. This highlights that the P sites are not simple spectators and provide moderate bonding to important intermediates involved in the HER. As a result, the rls, that is the removal of H_2 from $Ni_2P(001)$, becomes less energy-consuming (ΔE_{rls} =0.45eV), compared to the cases of Ni(111) and Pt(111). Overall, the catalytic activity of the $Ni_2P(001)$ surface towards the HER should be better than those of Pt (111) and Ni(111), but worse than those of the [NiFe] hydrogenase and the $[Ni(PNP)_2]^{2+}$ complex. A further study shows that the strong interaction of H with the Ni hollow sites can lead to poisoning of the most chemically active part of the surface under the real working conditions for the HER [13]. With the Ni hollow sites occupied, the HER on $Ni_2P(001)$ occurs at two Ni-P bridge sites, and the bonding to the first and second H atoms becomes endothermic. As a result, the H poisoning of the $Ni_2P(001)$ surface does not deactivate the catalyst at all; Instead, the cost for the rls (the addition of the second H) is lowered to 0.21eV.

Overall, DF calculations show that the $Ni_2P(001)$ surface should display a better catalytic activity toward the HER than the conventional catalyst Pt. Comparing to the [NiFe] hydrogenase and the analogue complexes ($[Ni(PS3*)(CO)]^{1-}$ and $[Ni(PNP)_2]^{2+}$), the HER on pure $Ni_2P(001)$ is less efficient, due to the fact that Ni sites of $Ni_2P(001)$ bond hydrogen too strongly hindering its removal from the surface. Different from the HDS catalysis [11], the weak ligand effect of P on Ni does not contribute to the good behavior of Ni_2P towards the HER. In fact, it is the ensemble

effect, which plays an essential role for the high activity of Ni_2P towards the HER. The energy cost for hydrogen removal (rls) from Ni_2P is decreased by binding the second H atom at the less active Ni-P bridge sites, rather than the Ni hollow sites, and the HER activity decreases follows the sequence: [NiFe] hydrogenase > $[Ni(PNP)_2]^{2+}$ > $[Ni(PS3*)(CO)]^{1-}$ > Ni_2P > Pt > Ni, according to the kinetic studies based on the DF calculations [13]. The promotion of Ni_2P towards the HER becomes more pronounced with H-poisoning, in which the reaction occurs over two Ni-P bridges sites with an efficiency comparable to that of the [NiFe] hydrogenase. In this case, the H-poisoning helps.

An important point in this study is that surfaces of pure transition metals do not have the necessary chemical properties for being highly active catalysts for hydrogen evolution. Such catalysts must have a moderate interaction with hydrogen species, combining proton-acceptor sites (negative charged non-metal atoms) and hydride-acceptor sites (isolated metal atoms) that work in a cooperative way. Given these requirements, even alloys of transition metals with inert metals (Cu, Ag, Au) may not work well, and the logical focus in the search for highly active HER catalysts should be on compounds of transition metal with light elements.

The water-gas shift reaction on extended metal surfaces and nanoparticles

The water-gas shift reaction (WGS: $CO + H_2O \rightarrow H_2 + CO_2$) is a critical process in providing pure hydrogen for fuel cells and other applications [41]. Improved air-tolerant, cost-effective WGS catalysts for lower temperature processing are needed to enable mobile fuel cell applications in a hydrogen fuel economy [42,43]. In the industry, mixtures of Fe-Cr and Zn-Al-Cu oxides are frequently used as catalysts for the water-gas shift reaction at temperatures between 350-500 and 180-250 C, respectively [41]. These oxide catalysts are pyrophoric and normally require lengthy

and complex activation steps before usage. Consequently other catalysts are being sought. Au-CeO_2 and Cu-CeO_2 nanocatalysts are very promising new candidates for high activity, lower temperature WGS systems [42,44,45]. However, the design and optimization of these or other metal/oxide nanocatalysts for the production of hydrogen through the WGS are hindered by controversy about basic questions regarding the nature of the active sites and the reaction mechanism. A key issue is the intrinsic ability of Cu and Au to catalyze the WGS process. DF calculations were carried out to study the WGS on periodic surfaces and nanoparticles of copper and gold [17,18].

The DF-calculated energy profile for the WGS on Au(100) and Cu(100) surfaces, including kinetic barriers, is shown in Figure 15 [18]. The energies are expressed with respect to the clean surface, a free CO molecule and two water molecules in the gas phase. On Cu(100), the first and the most energy-consuming step, or rate-limiting step (rls), is water dissociation with a ΔE_3 of +0.39eV and a barrier (ΔEa_3) of +1.13eV. In contrast, the dissociation of adsorbed OH and the formation of CO_2 are more facile. All the adsorbates bond more weakly on Au(100) than on Cu(100). Consequently, the rate-limiting dissociation of H_2O on Au(100) is even more endothermic (ΔE_3 = +0.74eV) and the corresponding barrier is also higher (ΔEa_3 = +1.53eV). These DF results are in good agreement with experimental measurements [17], which show that Cu is a good WGS catalyst while Au is an extremely poor one.

Can nanoparticles of Cu and Au catalyze the WGS reaction on their own without the aid of an oxide support? Are these nanoparticles more reactive than extended surfaces of the pure metals? Theoretical studies have shown that unsupported Au nanoparticles can be very active for the oxidation of CO [46]. On the other hand, results of DF calculations indicate that free Au clusters are not able to dissociate SO_2 [47]. DF calculations were utilized to investigate the

WGS reaction on Cu_{29} and Au_{29} clusters [18]. The Cu_{29} and Au_{29} clusters exhibited a pyramidal structure formed by the interconnection of (111) and (100) faces of the bulk metals, see Figure 16. It has three layers containing 16, 9 and 4 metal atoms. Similar Au clusters have been observed on CeO_2(111) with STM and on TiO_2 with TEM [17,46]. Figure 17 shows the calculated energy changes for the WGS reaction on a Cu_{29} cluster. The reaction pathway with the minimum energy barriers involves the following steps:

$$CO_{gas} \leftrightarrow CO_{ads} \quad (1)$$

$$H_2O_{gas} \leftrightarrow H_2O_{ads} \quad (2)$$

$$H_2O_{ads} \rightarrow OH_{ads} + H_{ads} \quad (3)$$

$$CO_{ads} + OH_{ads} \rightarrow OCOH_{ads} \quad (4)$$

$$OCOH_{ads} \rightarrow CO_{2,gas} + H_{ads} \quad (5)$$

$$2H_{ads} \rightarrow H_{2,gas} \quad (6)$$

The adsorption of CO or H_2O on the Cu particle is clearly exothermic. The first and most important energy barrier is for the dissociation of water into adsorbed OH and H. Then, the reaction of OH and CO produces a formate-like species (OCOH). The last important energy barrier is for the decomposition of the OCOH intermadiate into CO_2 gas and adsorbed H that eventually yields H_2 gas. The DF results indicate that a free Cu particle can catalyze the WGS reaction easily. A comparison to the corresponding results on Cu(100) shows that on the extended surface the dissociation of water has a larger activation barrier (1.13 eV *vs* 0.94 eV on the nanoparticle) and there is no formation of a stable OCOH intermediate since a redox mechanism operates [18]. The presence of corner or edge atoms in Cu_{29} favors the dissociation of H_2O and the formation of the OCOH species [17,18].

Theoretical calculations indicate that a Au_{29} cluster interacts well with atomic and molecular hydrogen [46]. However, it does not bond or dissociate the water molecule. We investigated the $H_2O \leftrightarrow Au_{29}$ interactions for all the adsorption sites shown in Figure 16 and in all cases we found no bonding. This can be contrasted with the case of a Cu_{29} cluster or a Cu(100) surface where the WGS reaction occurs readily [18]. Figure 18 shows a correlation between the calculated barrier (y-axis) and the calculated reaction energy (x-axis) for water dissociation on Au(100), Cu(100) as well as ionic and neutral Au_{29} and Cu_{29} nanoparticles [17]. All the gold systems are characterized by a large activation barrier and an endothermic ΔE. When going from Au(100) to Au_{29} there is a significant improvement in chemical reactivity, but it is not enough for dissociating the water molecule. Charging of the Au nanoparticle to form either Au_{29}^- or Au_{29}^+ also does not help [17]. These results cannot explain the large catalytic activity seen for Au-CeO_2 or Au-MoO_2 catalysts [17,48] and highlight the important role of the oxide in the activation of the system. The oxide support could activate the system by modifying the electronic properties of the metal nanoparticles or by participating directly in the WGS reaction (i.e dissociation of the water molecule) [17,48].

Recent experiments have found that Mo_2C is an attractive candidate for replacing Cu-based catalysts in automotive vehicles powered by fuel cells because it shows a higher activity and stability during the WGS reaction [49,50]. However, the underlying mechanism of the WGS reaction still remains elusive. DF and a micro-kinetic model were used to study the WGS reaction on Mo_2C(001) surfaces [51]. The DF results showed that the WGS reaction follows a redox mechanism in which successive oxidation and reduction of the surface occurs. The activity of the carbides decreases in a sequence: Cu(111) > C-terminated Mo_2C(001) (C-Mo_2C) > Mo-terminated Mo_2C(001) (Mo-Mo_2C). Both Mo_2C and C-Mo_2C are less reactive than the

conventional WGS catalyst, Cu. This is due to the fact that either the Mo sites or the C sites bond oxygen too strongly to allow the facile removal of oxygen and lead to O-poisoning. The O-covered Mo-terminated $Mo_2C(001)$ (O_Mo-Mo_2C) is the worst case. Although the O-covering results in a weakening of the O-surface interaction, O_Mo-Mo_2C is too inert to adsorb CO and dissociate H_2O. In contrast, the C-Mo_2C covered by the same amount of oxygen (O_C-Mo_2C) displays the highest WGS activity of all. Overall, the high WGS activity observed experimentally is due to the formation of a Mo oxocarbide in the surface of $Mo_2C(001)$ during the WGS reaction. The C atoms destabilize the covered O by forming CO species, which shift away from the Mo hollow sites when the surface reacts with other adsorbates. In this way, the Mo sites are able to bond the reaction intermediates moderately, which results in a high WGS activity. In addition, both C and O atoms are not spectators and directly participate in the WGS reaction [51].

Conclusion

Advances in theoretical methods (mainly based on density functional theory) make possible to study nowadays, in a quantitative or semi-quantitative way, a series of phenomena associated with heterogeneous catalysis. In several cases this has led to a fundamental understanding of catalytic processes. However, many problems in this complex area remain as a challenge, and the approximate nature of most theoretical methods makes necessary a close coupling of theory with experiment. This multidisciplinary approach can provide a conceptual framework for modifying or controlling the main parameters affecting catalytic reactions. In this respect, theoretical calculations can be very useful for predicting the best ways for enhancing the performance of existing catalysts or for designing new ones in a rational way.

Acknowledgements

In the past years a great number of people in the Catalysis Group at BNL have been helpful in discussing many problems associated with desulfurization reactions and the production of hydrogen. Special thanks to J. Hanson, J. Hrbek, J. Lightstone, J. Muckerman, X. Wang, W. Wen and M. White. We are also grateful to J. Evans and M. Pérez from the Universidad Central of Venezuela for thought provoking conversations. The work carried out at Brookhaven National Laboratory was supported by the US Department of Energy under contract DE-AC02-98CH10086.

REFERENCES

1. G. Ertl, H. Knözinger, and J. Weitkamp (Editors), *Handbook of Heterogeneous Catalysis*, Wiley-VCH: Weinheim.
2. J.M. Thomas and W.J. Thomas, Principles and Practice of Heterogeneous Catalysis, VCH, New York, 1997.
3. B. Hammer and J.K. Nørskov, Adv. Catal. 45 (2000) 71.
4. J.A. Rodriguez, Theoretical Chem. Accounts, 107 (2002) 117-129.
5. J.L. Whitten and H. Yang, Surf. Sci. Report, 24 (1996) 55.
6. R.A.van Santen and M. Neurock, Catal. Rev. Sci.-Eng. 37 (1995) 557.
7. R.A. van Santen and M. Neurock, *Molecular Heterogeneous Catalysis: A Conceptual*

and Computational Approach, Wiley-VCH, New York, 2006.

8 J.A. Rodriguez and D.W. Goodman, Surf. Sci. Reports 14 (1991) 1.

9. G.A. Somorjai, *Introduction to Surface Chemistry and Catalysis*, Wiley, New York, 1994.

10. I. Chorkendorff and J.W. Niemantsverdriet, *Concepts of Modern Catalysis and Kinetics*, 2nd Edition, Wiley-VCH, New York, 2007.

11. P. Liu, J.A. Rodriguez, T. Asakura, J. Gomes, K. Nakamura, J. Phys. Chem. B, 109 (2005) 4575.

12. P. Liu, J. A. Rodriguez and J. T. Muckerman, J. Phys. Chem. B, 108 (2004) 15662.

13. P. Liu and J.A. Rodriguez, J. Am. Chem. Soc. 127 (2005) 14871.

14. J.A. Rodriguez, P. Liu, J. Dvorak, T. Jirsak, J. Gomes, Y. Takahashi, K. Nakamura, Phys. Rev. B, 69 (2004) 115414.

15. P. Liu, J.A. Rodriguez, J.T. Muckerman, J. Phys. Chem. B, 108 (2004) 18796.

16. P. Liu, J.A. Rodriguez and J.T. Muckerman, J. Molecular Catal. A: Chemical, 239 (2005) 116.

17. J.A. Rodriguez, P. Liu, J. Hrbek, J. Evans and M. Perez, Angew. Chem. Int. Ed. 46 (2007) 1329.

18. P. Liu and J.A. Rodriguez, J. Chem. Phys. 126 (2007) 164705.

19. E. Furimsky, Applied Catal. A: General, 240 (2003) 1.

20. K.A. Layman, M.E. Bussell, J. Phys. Chem. B, 108 (2004) 15791.

21. J.G. Speight, The Chemistry and Technology of Petroleum, 2nd Ed, Dekker, New York, 1991.

22. H. Topsøe, B.S. Clausen and F.E. Massoth, *Hydrotreating Catalysis: Science and*

Technology, Springer, Heidelberg, 1996.

23. B. Diaz, S.J. Sawhill, D.H. Bale, R. Main, D.C. Phillips, S. Korlann, R. Self, and M.E. Bussell, Catal. Today, 86 (2003) 191.
24. P. Liu, J.A. Rodriguez, J. Chem. Phys. 120 (2004) 5414.
25. T.P. St. Clair, S.T. Oyama, D.F. Cox, Surf. Sci. 511 (2002) 294.
26. J.A. Rodriguez, J.Y. Kim. J.C. Hanson. S.J. Sawhill, M.E. Bussell, J. Phys. Chem. B, 107 (2003) 6276.
27. S.J. Sawhill, D.C. Phillips, and M.E. Bussell, J. Catal. 215 (2003) 208.
28. D. Kanama, S.T. Oyama, S. Otani, and D.F. Cox, Surf. Sci. 552 (2004) 8.
29. K. Christmann, *Frontiers in Electrochemistry*, Lipkowski, J.; Ross, P.N. ed.; Vol. 1, Wiley, New York, 1998.
30. C. Tard, X.M. Liu, S.K. Ibrahim, M. Bruschi, L. De Gioia, S.C. Davies, X. Yang, L.S. Wang, G. Sawers, and C.J. Pickett, Nature 433 (2005) 610.
31. S. E. Lamle, S. P. J. Albracht, and F. A. Armstrong, J. Am. Chem. Soc. 127 (2005) 6595.
32. P.E.M. Siegbahn, Adv. Inorg. Chem. 56 (2004) 101.
33. P. Amara, A. Volbeda, J.C. Fontecilla-Camps, M.J. Field, J. Am. Chem. Soc. 121 (1999) 4468.
34. S. Ott, M. Kritikos, B. Akermark, L.C. Sun, and R. Lomoth, Angew. Chem. Intl. Ed. 43 (2004) 1006.
35. S.J. Borg, T. Behrsing, S.P. Best, M. Razavet, X.M. Liu, and C.J. Pickett, J. Am. Chem. Soc. 126 (2004) 16988.
36. B. Hinnemann, P.G. Moses, J. Bonde, K.P. Jørgensen, J.H. Nielsen, S. Horch, I. Chorkendorff, J.K. Nørskov, J. Am. Chem. Soc. 127 (2005) 5308.

37. P. Amara, A. Volbeda, J.C. Fontecilla-camoes, and M.J. Field, J. Am. Chem. Soc. 121 (1999) 4468.

38. C. Stadler, A.L. de Lacey, Y. Montet, A. Volbeda, A. Vernede, J.C. Fontecilla-camoes, J.C. Conesam, and V.M. Fernandez, Inorg. Chem. 41 (2002) 4424.

39. V.G.H. Eijsink, A. Bjørk, S. Gåseidnes, R. Sirevåg, B. Synstad, B. van den Burg, and G. Vriend, J. Biotechnol. 113 (2004) 105.

40. A. Korkegain, M.E. Black, D. Baker, and B.L. Stoddard, Nature 308 (2005) 857.

41. K. Klier, C.W. Young, J.G. Nunan, Industrial & Engineering Chemistry Fundamentals 25 (1986) 36-42.

42. Q. Fu, H. Saltsburg, M. Flytzani-Stephanopoulos, Science 301 (2003) 935-938.

43. G. Germani, Y. Schuurman, Aiche Journal 52 (2006) 1806-1813.

44. X. Wang, J.A. Rodriguez, J.C. Hanson, M. Pérez and J. Evans, J. Chem. Phys. 123 (2005) 221101.

45. X. Wang, J.A. Rodriguez, J.C. Hanson, D. Gamarra, A. Martínez-Arias, and M. Fernández-García, J. Phys. Chem. B, 110 (2006) 428.

46. L. Barrio, P. Liu, J.A. Rodriguez, J.M. Campos-Martin, and J.L.G. Fierro, J. Chem. Phys. 125 (2006) 164715.

47. J.A. Rodriguez, M. Pérez, T. Jirsak, J. Evans, J. Hrbek, and L. González, Chem. Phys. Lett. 378 (2003) 526.

48. J.A. Rodriguez, P. Liu, J. Hrbek, J. Evans and M. Perez, J. Molec. Catal. A, in press.

49. D.J. Moon, and J. W. Ryu, Catal. Lett. 92 (2004) 17.

50. J. Patt, D. J. Moon, C. Phillips, and L. Thompson, Catal Letters 65 (2000) 193.

51. P. Liu, and J.A. Rodriguez, Journal of Physical Chemistry B 110 (2006) 19418

Figure captions

Figure 1 Top a side views for α-Mo_2C(001) and MoC(001) surfaces and for a metcar Mo_8C_{12} nanoparticle. Blue spheres denote Mo atoms, while C atoms are shown as grey spheres.

Figure 2 Top panel: Calculated Mulliken charges for Mo atoms in α-Mo_2C(001), MoC(001) and a metcar Mo_8C_{12}. Bottom panel: Corresponding variation in the centroid of the Mo 4d band (taken from ref. [24]).

Figure 3 Calculated bonding energies for a S atom on Mo(110), α-Mo_2C(001), MoC(001) and a metcar Mo_8C_{12} (taken from ref. [12]).

Figure 4 Adsorption geometry calculated for thiophene on a α-Mo_2C(001) surface (taken from ref. [12]).

Figure 5 Adsorption geometry calculated for thiophene on a MoC(001) surface (taken from ref. [12]).

Figure 6 Optimized structures for a thiophene + $3H_2$ → C_4H_8 + H_2S reaction on Ti_8C_{12} (taken from ref. [15]).

Figure 7 Calculated ΔE's and activation energies for the HDS process shown in Figure 6 (taken from ref. [15]).

Figure 8 Structure of the Ni_2P(001) surface. The dark blue spheres denote Ni atoms, P atoms are represented by soft purple spheres (taken from ref. [11]).

Figure 9 Calculated ΔE's for the thiophene + $2H_2$ → C_4H_6 + H_2S reaction on Ni_2P(001) (taken from ref. [11]).

Figure 10 Calculated energy changes for the HER on the [NiFe] hydrogenase, the $[Ni(PS3^*)(CO)]^{1-}$ and $[Ni(PNP)_2]^{2+}$ complexes , plus Ni_2P(001), Pt(111) and Ni(111)

surfaces. The energy change for the $2(H^+ + e^-) \rightarrow H_2$ reaction is defined as zero by setting the reference potential to be that of the standard hydrogen electrode. In the figure we are plotting relative energy changes with respect to this zero of reference (taken from ref. [13]).

Figure 11 Optimized structures for each step in a catalytic cycle for the HER on the [NiFe] hydrogenase (taken from ref. [13]). White: H; Grey: C; Navy: Ni; Cyan: Fe; Blue: N; Red: O; Yellow: S.

Figure 12 Optimized structures for each step in a catalytic cycle for the HER on the $[Ni(PS3^*)(CO)]^{1-}$ complex (taken from ref. [13]). White: H; Grey: C; Navy: Ni; Purple: P; Blue: N; Red: O; Yellow: S.

Figure 13 Optimized structures for each step in a catalytic cycle for the HER on the $[Ni(PNP)_2]^{2+}$ complex (taken from ref. [13]). White: H; Grey: C; Navy: Ni; Purple: P; Blue: N.

Figure 14 Optimized structures for each step in a catalytic cycle for the HER on a $Ni_2P(001)$ surface (taken from ref. [13]). White: H; Navy: Ni; Purple: P.

Figure 15. Calculated energy profile for the WGS on Au(100) and Cu(100) surfaces (taken from ref. [18]).

Figure 16. Structure for Cu_{29} and Au_{29} nanoparticles seen on oxide surfaces [17,18].

Figure 17. Reaction profile and structures for the WGS reaction on a Cu_{29} nanoparticle. The zero energy is taken as the sum of the energies for the bare nanoparticle, gas-phase water and carbon monoxide. The red bars represent the transition state, and the black stand for reactants, intermediates or products. Yellow balls: Cu; red balls: O; grey balls: C; white balls: H. Cluster side view (taken from ref. [17]).

Figure 18. Correlation between the calculated barrier (y-axis) and the calculated reaction energy (x-axis) for water dissociation on Au(100), Cu(100) as well as ionic and neutral Au_{29} and Cu_{29} nanoparticles (taken from refs. [17,18]).

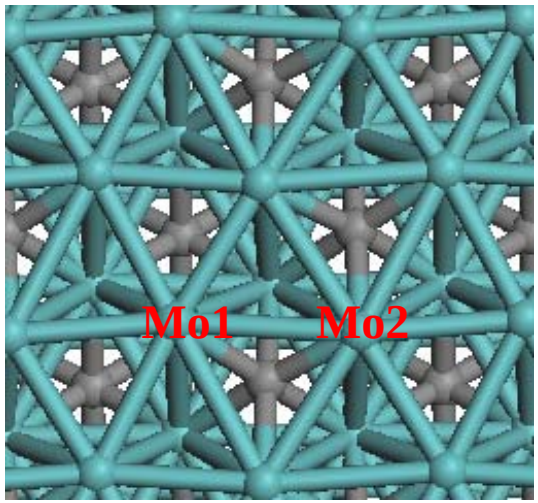

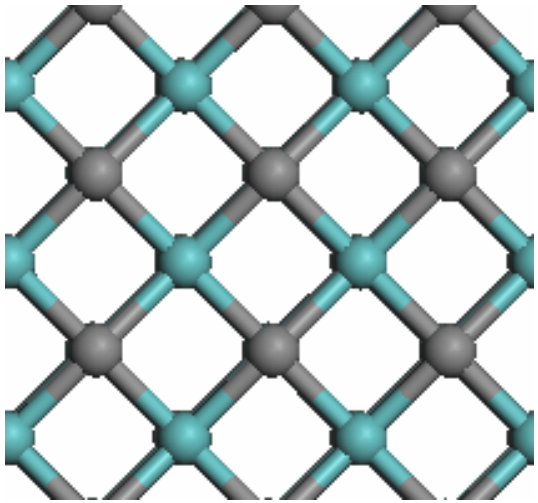

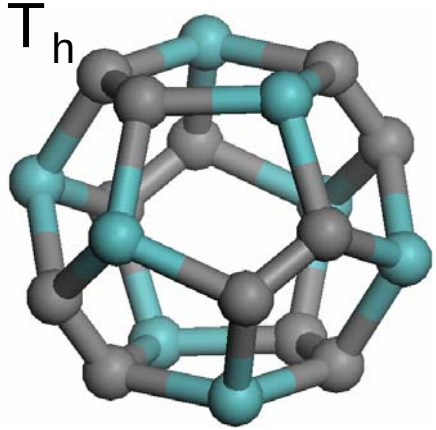

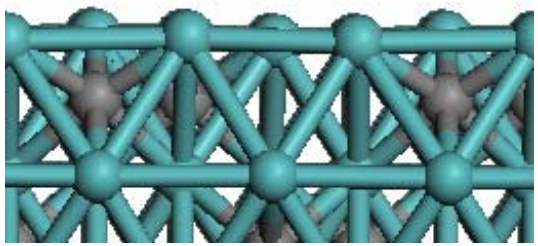

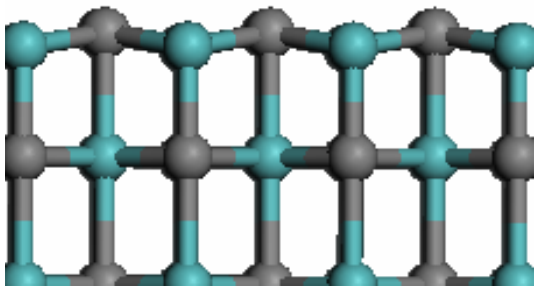

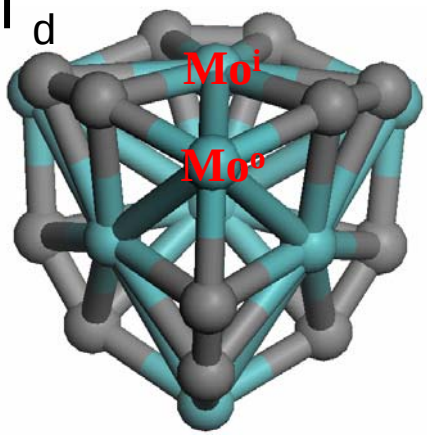

α-Mo_2C(001)

δ-MoC(001)

Mo_8C_{12}

Fig 1

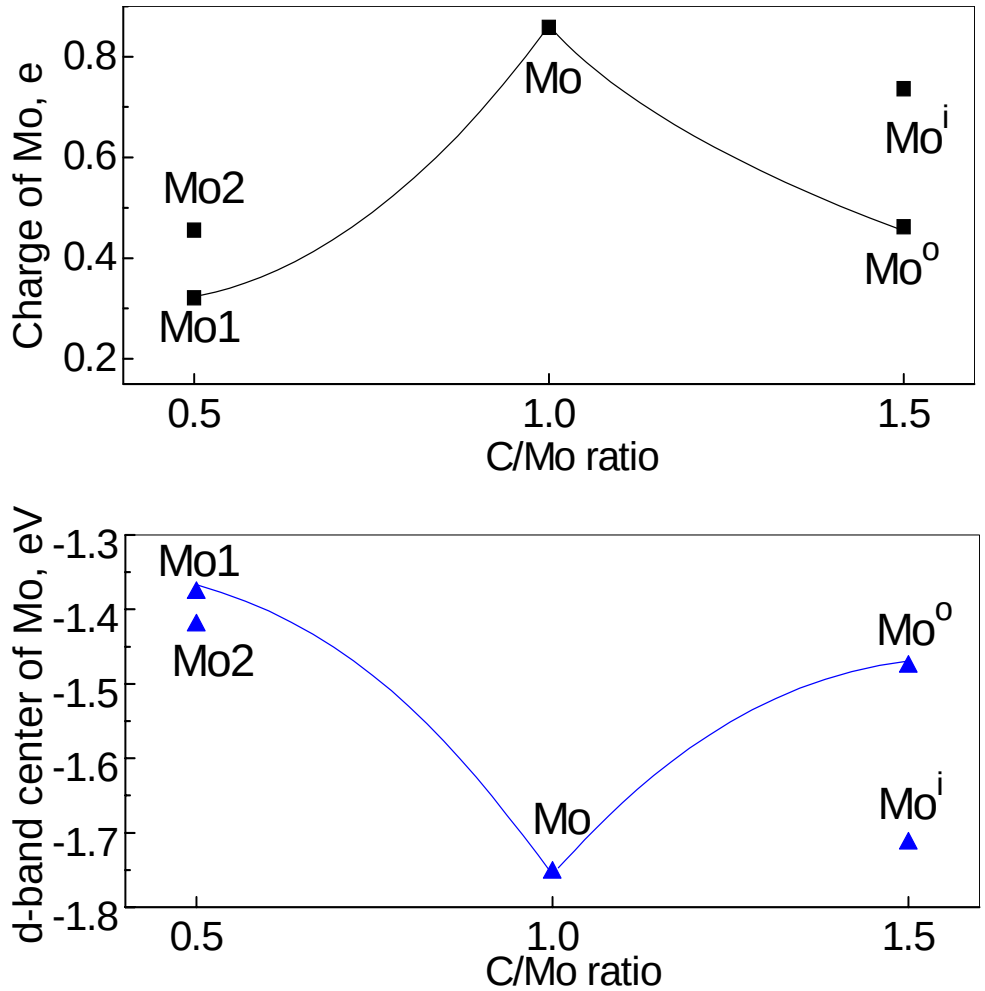
Charge of Mo, e
0.8
0.6
0.4
0.2
Mo
Mo2
Mo1
Mo^i
Mo^o
0.5
1.0
1.5
C/Mo ratio
d-band center of Mo, eV
-1.3
-1.4
-1.5
-1.6
-1.7
-1.8
Mo1
Mo2
Mo
Mo^o
Mo^i
0.5
1.0
1.5
C/Mo ratio

Fig 2

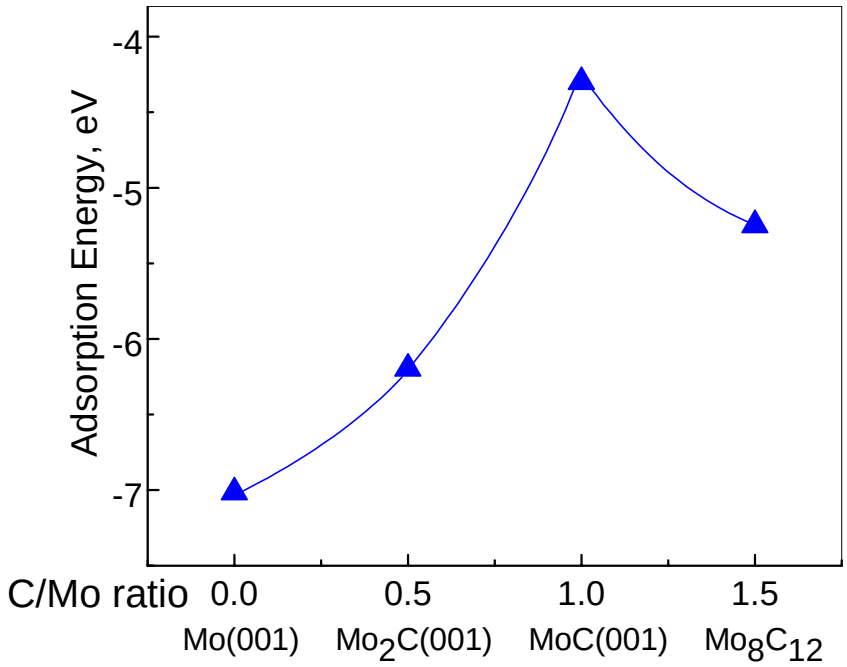
Adsorption Energy, eV
-4
-5
-6
-7
C/Mo ratio
0.0
0.5
1.0
1.5
Mo(001)
Mo2C(001)
MoC(001)
Mo8C12

Fig 3

Mo

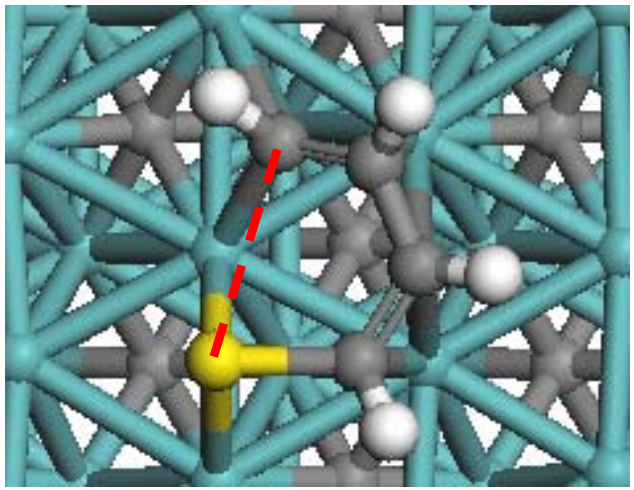

Top view

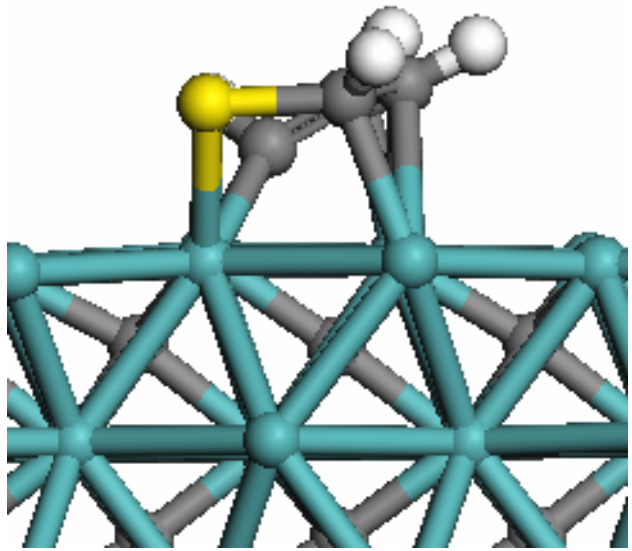

Side view

Fig 4

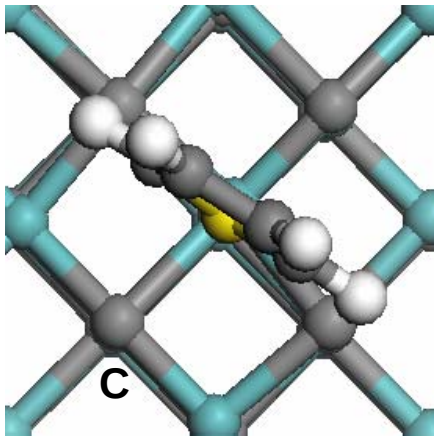

Top view

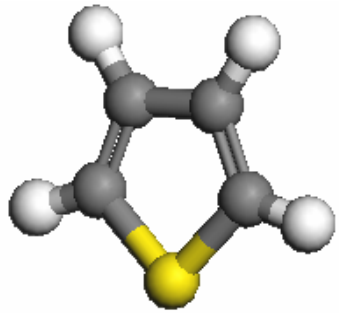

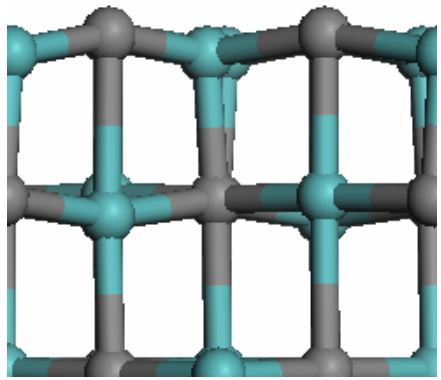

Side view

Fig 5

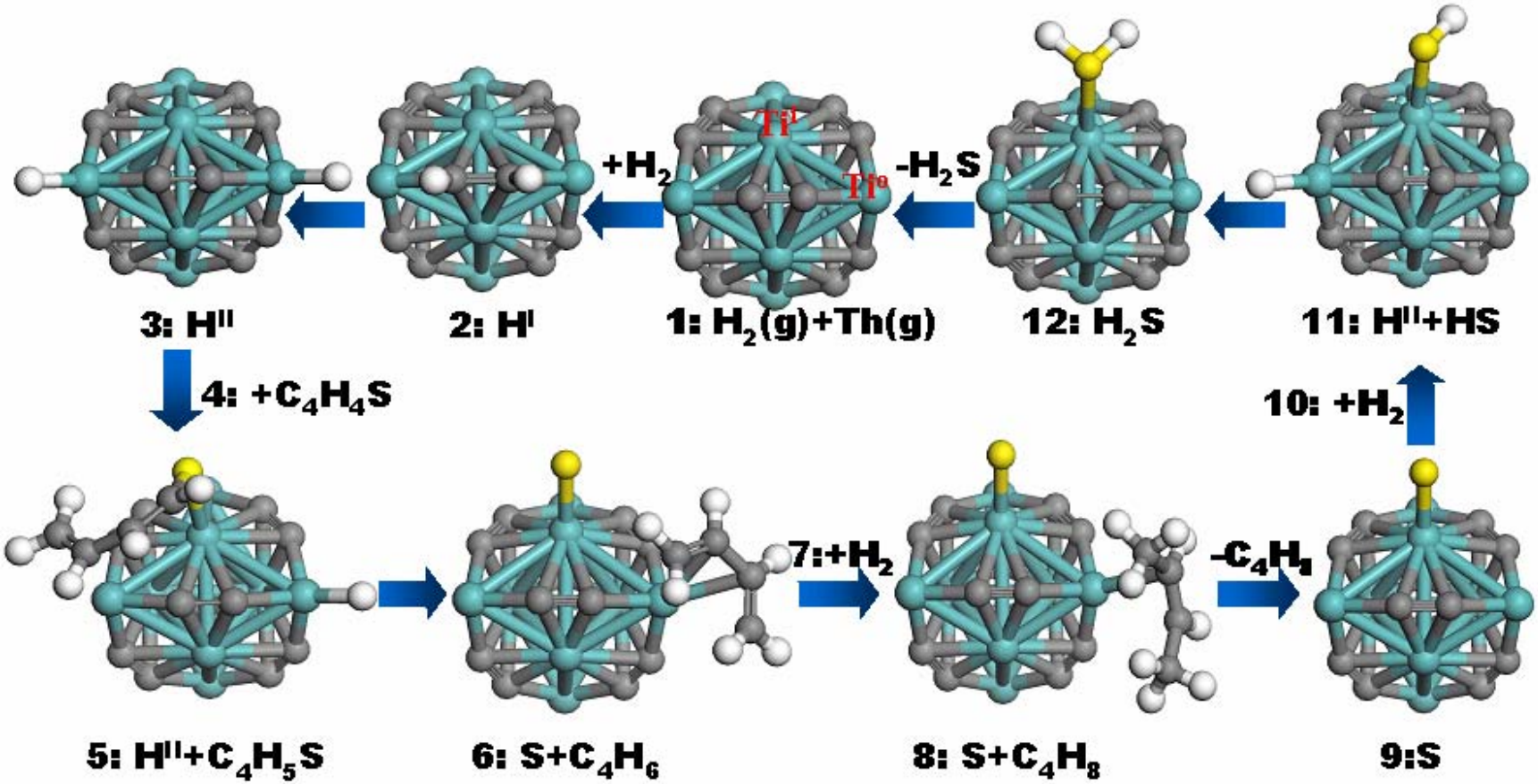

$$\text{Thiophene} + 3H_2 \longrightarrow C_4H_8 + H_2S$$

Fig 6

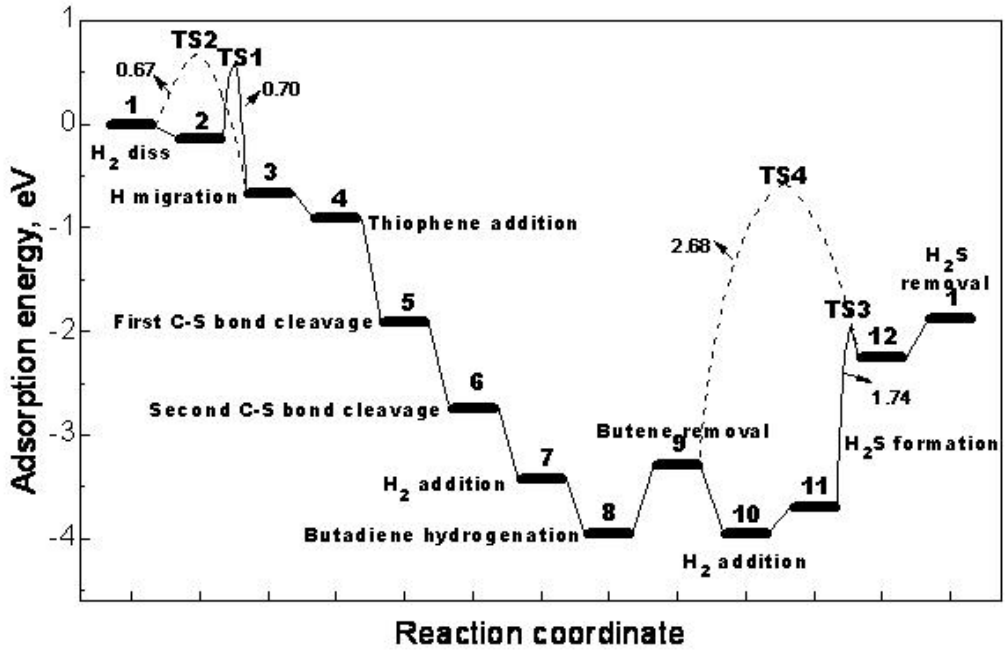
Adsorption energy, eV
Reaction coordinate
1
0
-1
-2
-3
-4
TS2
TS1
0.67
0.70
1
2
H2 diss
3
H migration
4
Thiophene addition
5
First C-S bond cleavage
6
Second C-S bond cleavage
7
H2 addition
8
Butadiene hydrogenation
9
Butene removal
TS4
2.68
10
H2 addition
11
H2S formation
TS3
12
1.74
H2S removal
1

Fig 7

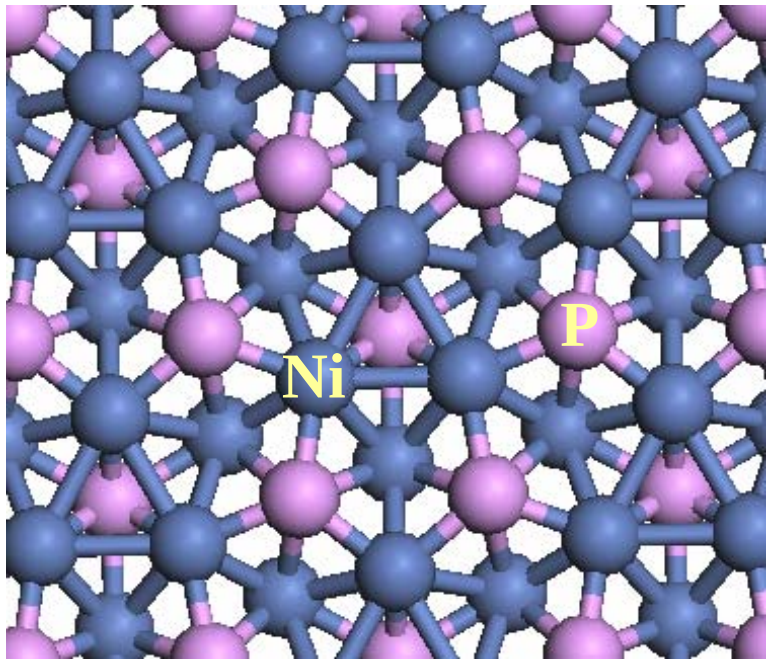

$Ni_2P(001)$

Fig 8

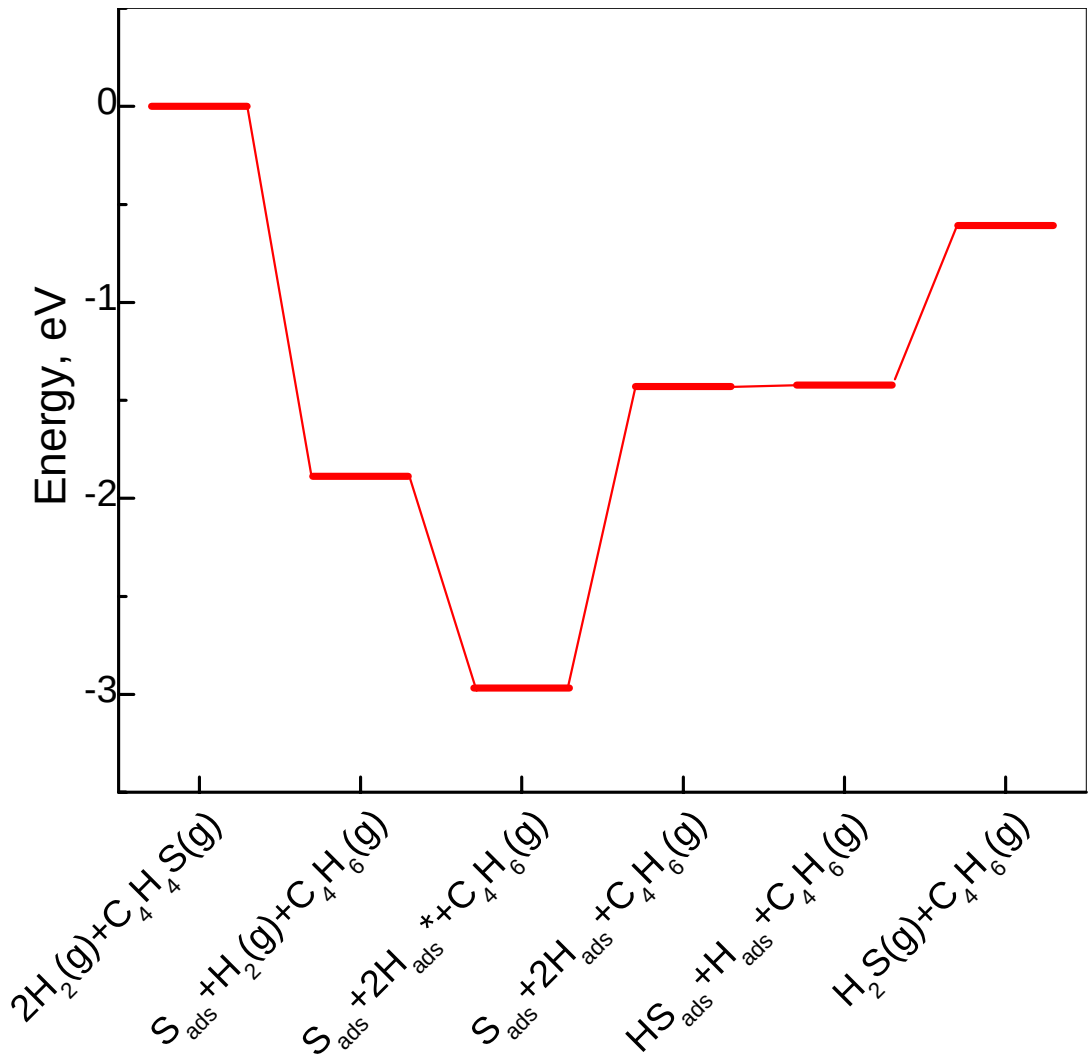
Energy, eV
0
-1
-2
-3
2H2(g)+C4H4S(g)
Sads +H2(g)+C4H6(g)
Sads +2Hads *+C4H6(g)
Sads +2Hads +C4H6(g)
HSads +Hads +C4H6(g)
H2S(g)+C4H6(g)

Fig 9

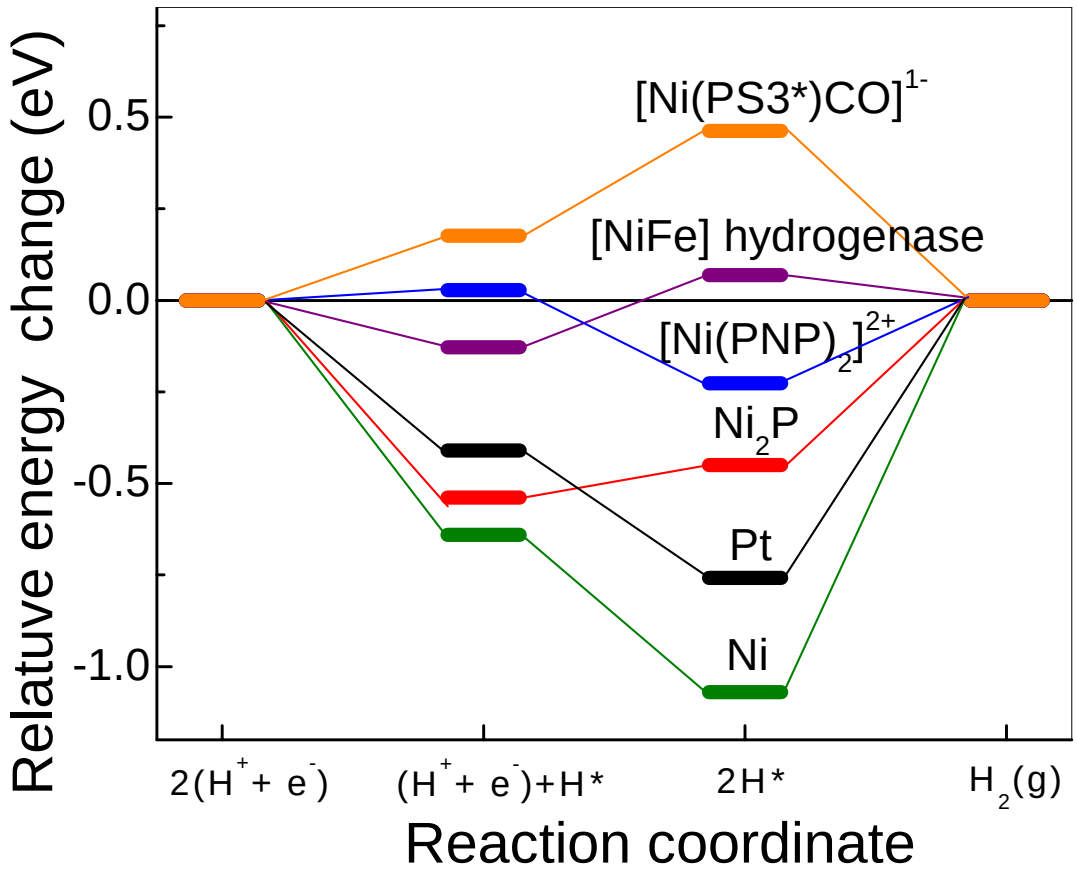
Relatuve energy change (eV)
0.5
0.0
-0.5
-1.0
[Ni(PS3*)CO]1-
[NiFe] hydrogenase
[Ni(PNP)2]2+
Ni2P
Pt
Ni
2(H+ + e-)
(H+ + e-)+H*
2H*
H2(g)
Reaction coordinate

Fig 10

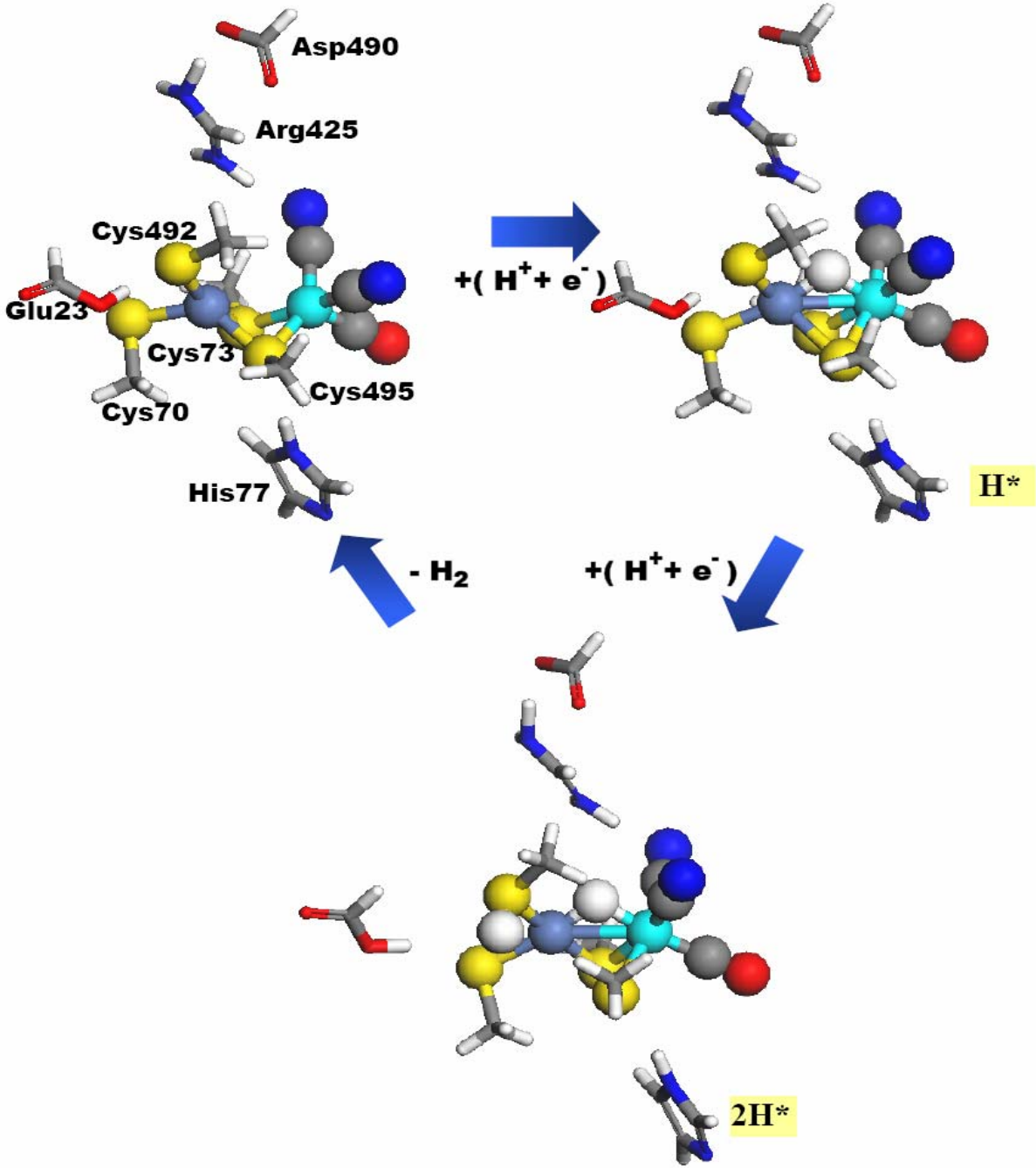
Asp490
Arg425
Cys492
Glu23
Cys73
Cys495
Cys70
His77
+(H+ + e-)
H*
+(H+ + e-)
- H2
2H*

Fig 11

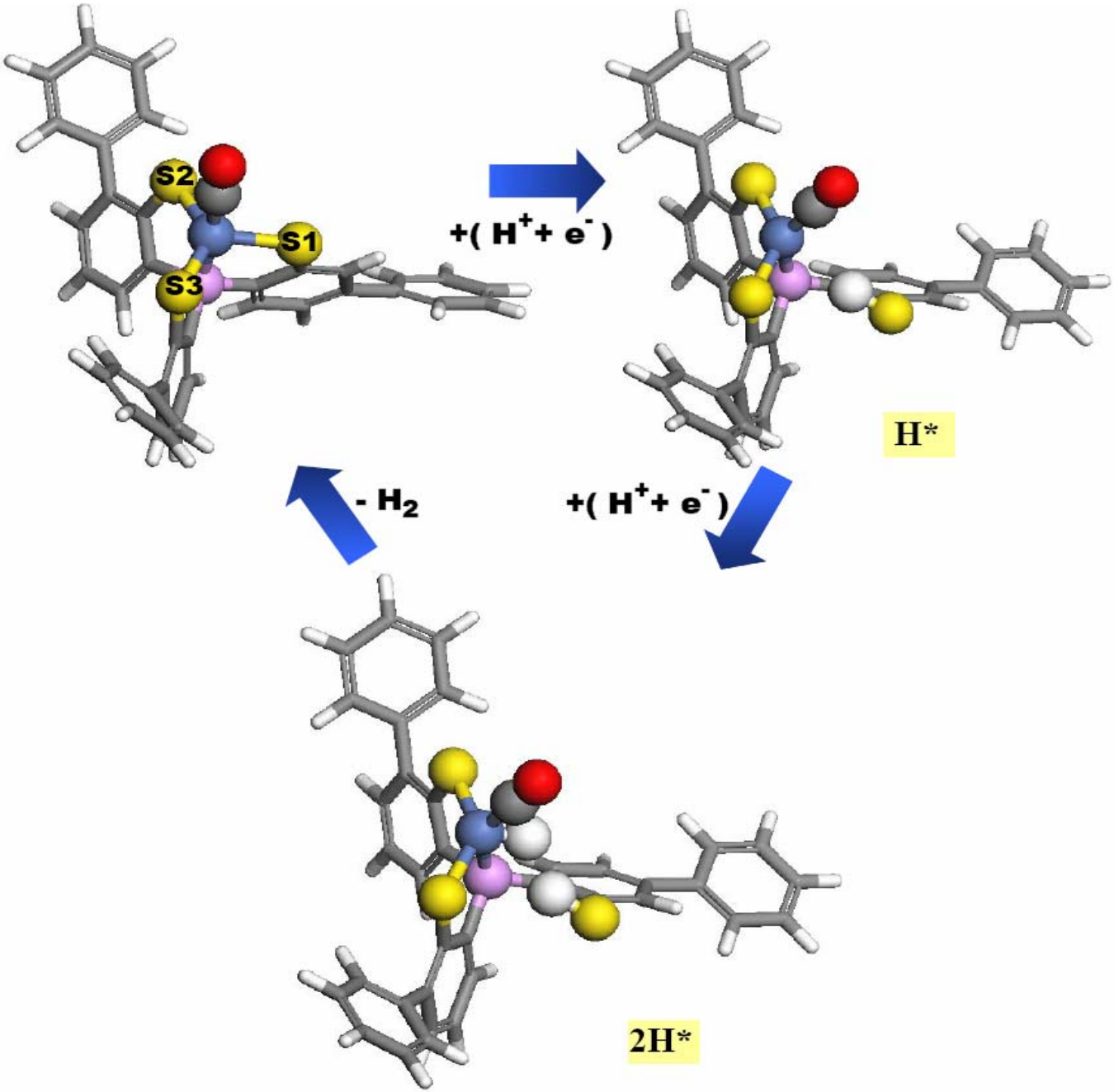

Fig 12

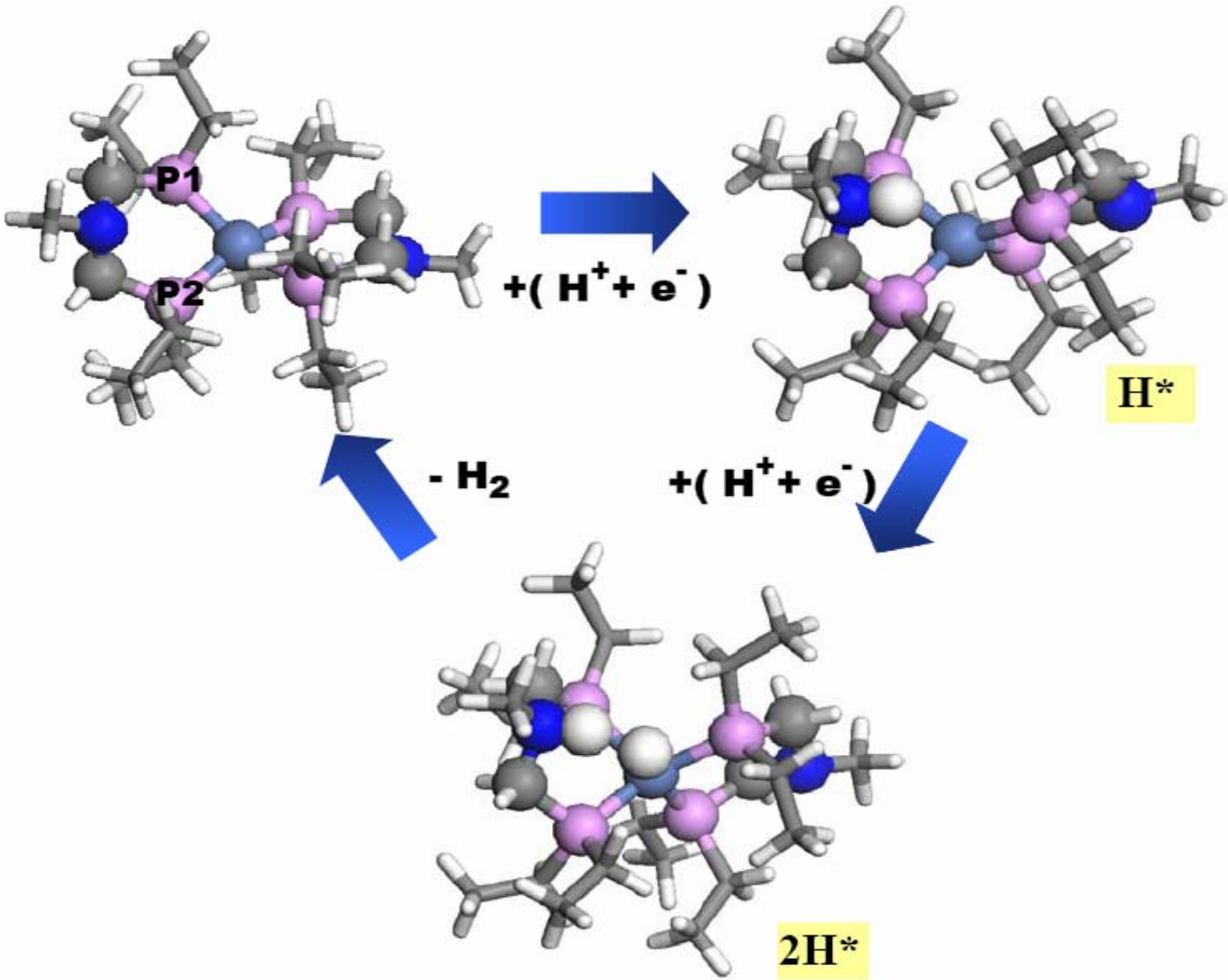

Fig 13

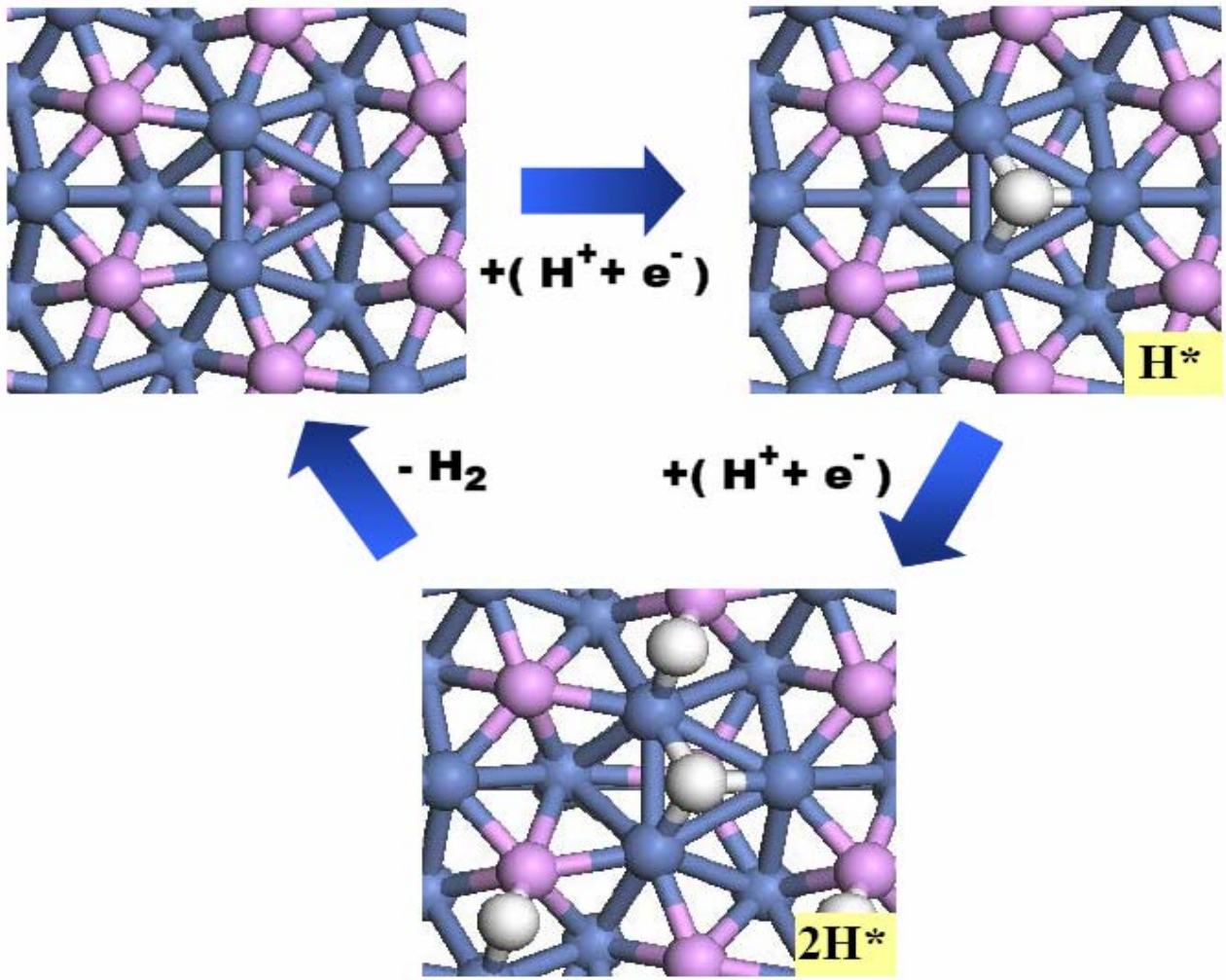

Fig 14

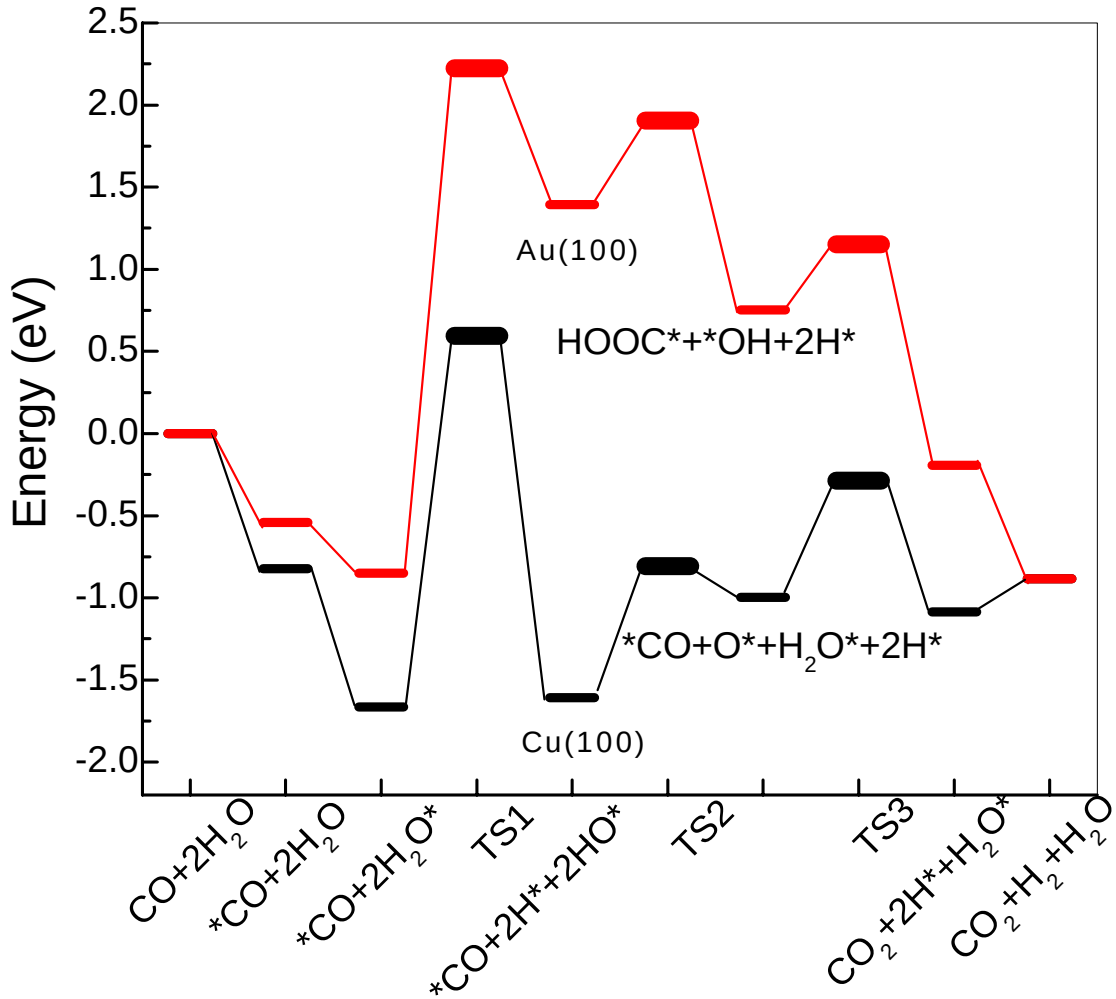
Energy (eV)
2.5
2.0
1.5
1.0
0.5
0.0
-0.5
-1.0
-1.5
-2.0
Au(100)
HOOC*+*OH+2H*
CO+O+H2O*+2H*
Cu(100)
CO+2H2O
*CO+2H2O
CO+2H2O
TS1
CO+2H+2HO*
TS2
TS3
CO2+2H*+H2O*
CO2+H2+H2O

Fig 15

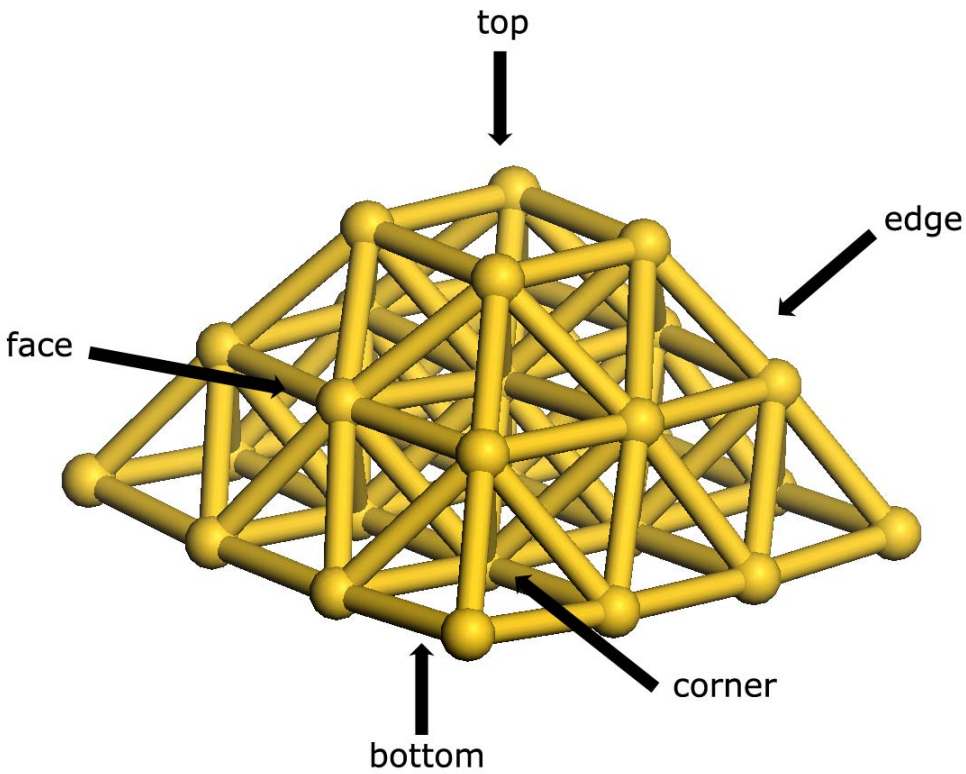

Fig 16

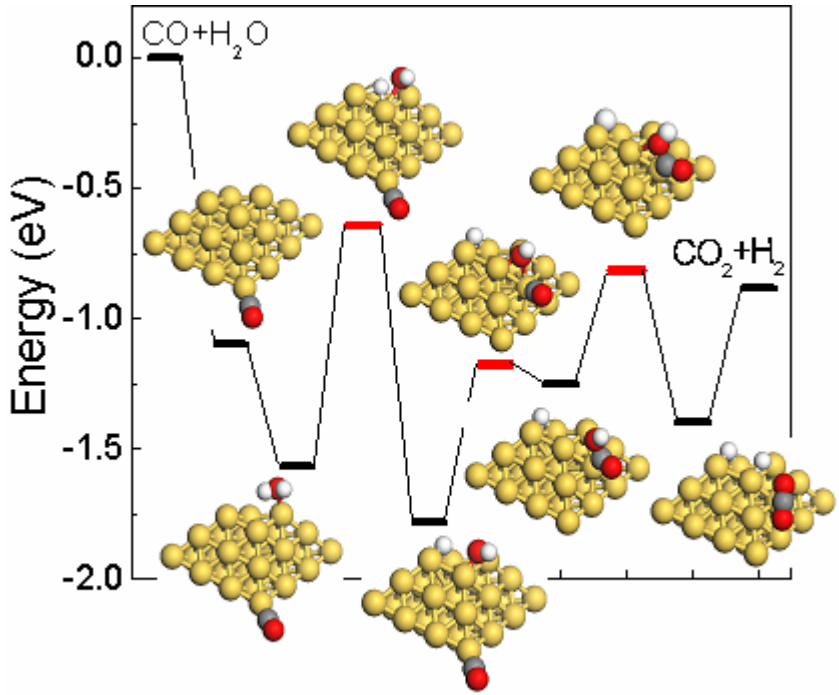

Fig 17

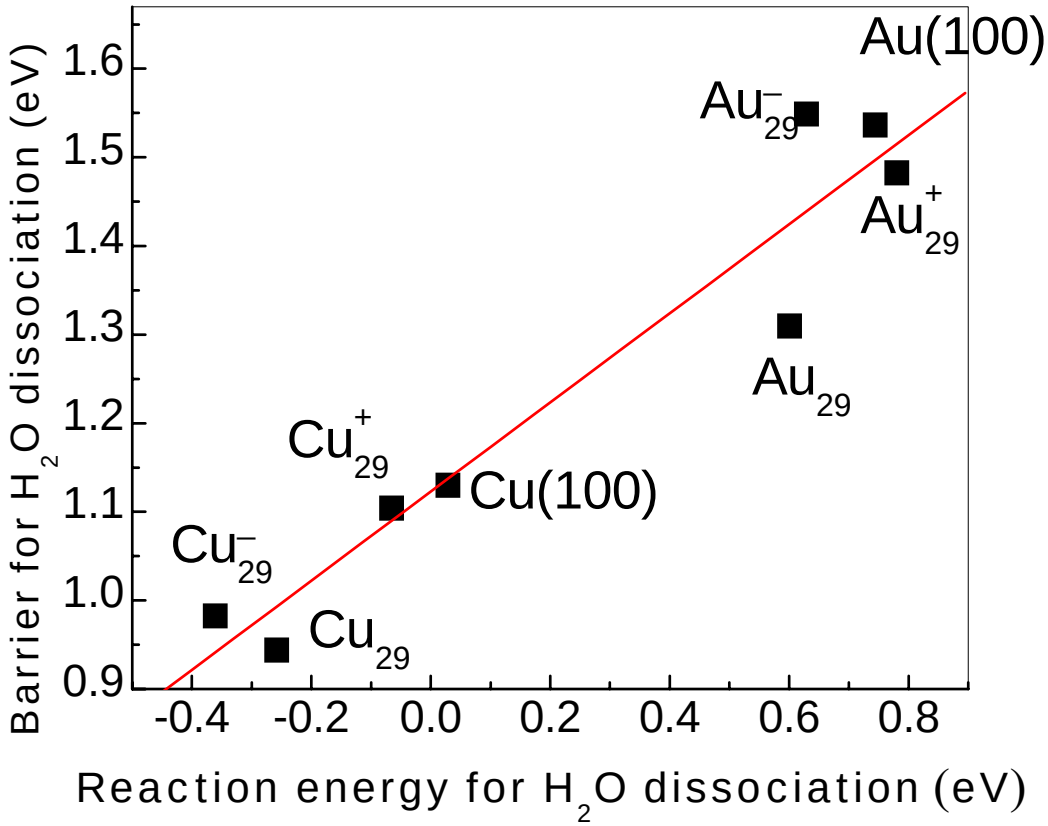
Au(100)
Au^-_{29}
Au^+_{29}
Au_{29}
Cu^+_{29}
Cu(100)
Cu^-_{29}
Cu_{29}
Barrier for H_2O dissociation (eV)
Reaction energy for H_2O dissociation (eV)
1.6
1.5
1.4
1.3
1.2
1.1
1.0
0.9
-0.4
-0.2
0.0
0.2
0.4
0.6
0.8

Fig 18

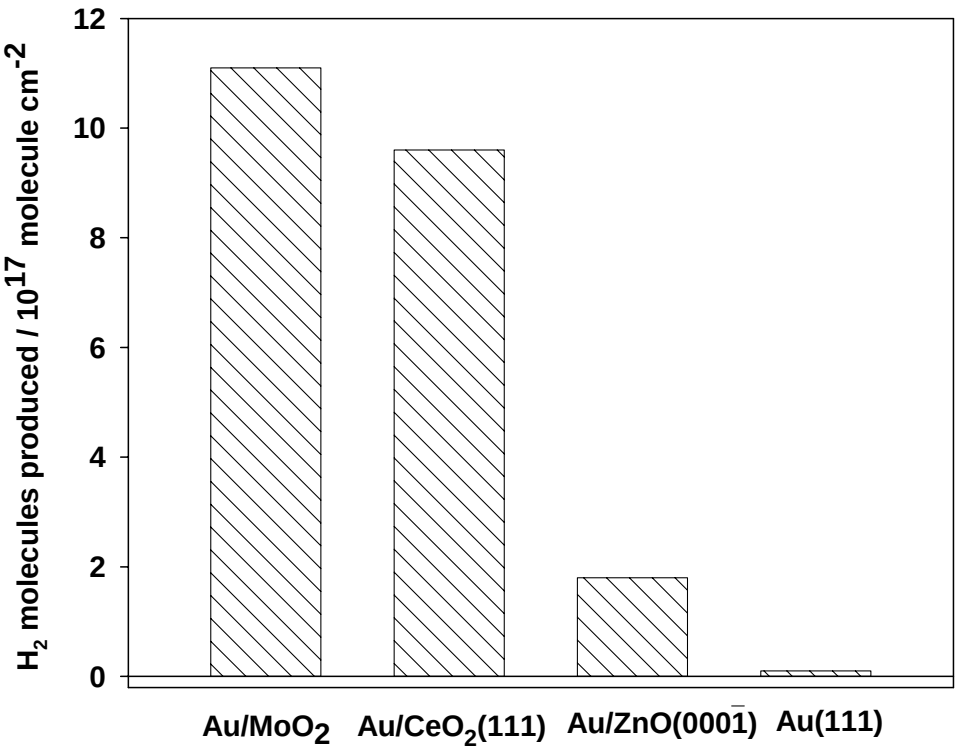
12
10
8
6
4
2
0
H_2 molecules produced / 10^{17} molecule cm^{-2}
Au/MoO_2
Au/CeO_2(111)
Au/ZnO(000$\bar{1}$)
Au(111)

Fig 19